ILASS–Europe 2019, 29th Conference on Liquid Atomization and Spray Systems, 2-4 September 2019, Paris, France

Towards lattice Boltzmann simulation of flow dynamics inside a model fuel injector: a first-stage study

Tianpei Luo[1,2,3], Jiaxian Zhang[1,3], Jun Xia[*,2], Yangwei Liu[*,4], Ruimin Liu[1,3], Sifeng Yang[1,3], Hua Zhao[2]

[1] Beijing Institute of Aerospace Testing Technology, Beijing 100074, China

[2] Department of Mechanical and Aerospace Engineering & Institute of Energy Futures, Brunel University London, Uxbridge UB8 3PH, UK

[3] Beijing Engineering Research Center of Aerospace Testing Technology and Equipment, Beijing 100074, China

[4] National Key Laboratory of Science and Technology on Aero-Engine Aero-Thermodynamics, School of Energy and Power Engineering, Beihang University, Beijing 100191, China

*Corresponding authors: jun.xia@brunel.ac.uk; liuyangwei@buaa.edu.cn

Abstract

Inside-fuel-injector flow conditions, such as injection pressure and gas-liquid two-phase cavitation flow dynamics, greatly affect fuel spray development and spray combustion performance of liquid-fuelled engine. The topic has attracted great interest for a long time. Measurement, however, has proven difficult due to harsh testing conditions on high pressure and flow velocity. On the other hand, computational approaches, which may play an important role in providing a detailed picture of inside-injector flow physics, are also limited due to the complexity of the needle movement and cavitating gas-liquid two-phase flow in the methodological framework of Navier-Stokes equations. Over the past three decades, the mesoscopic lattice Boltzmann method (LBM) [1] has attracted great attention due to its simple scheme, easement of dealing with complex geometry and convenience of parallel computing. Its mesoscopic nature makes it greatly suitable for simulating multiphase and multi-species flow. LBM can also effectively collaborate with the immersed boundary method [2, 3], since both approaches are usually discretised on regular Cartesian mesh, to deal with moving geometries in the computational domain. The clear advantages of the LBM over conventional approaches have motivated us to develop the approach for its applications in inner-injector flow, and a first-stage study is reported in this paper. First, an oscillating cylinder which moves with a sine function algorithm is simulated to model needle movement by using the immersed boundary method. Second, the Shan-Chen multiphase flow model [4, 5, 6] is employed to model both a spinodal decomposition case and an inside-nozzle flow in which cavitation emerges at the throating region of the model nozzle. It has been shown that both the immersed boundary method and the Shan-Chen model produce satisfactory results. Following the first-stage validation, we aim to further develop the LBM in collaboration with the immersed boundary method and Shan-Chen model to investigate flow dynamics inside a fuel injector where multiphase flow interacts with moving geometry.

Keywords

Fuel injector; Lattice Boltzmann; Moving geometry; Cavitation.

Introduction

The liquid-fuel injector is a key component of diesel engine, and the internal-flow dynamics inside a fuel injector has significant impact on the subsequent spray development and spray combustion performance including fuel consumption and exhaust emissions [7, 8]. So, the improvement of the nozzle design has been one of the major engine research areas over the years. Current fuel injection systems operate at very high pressures and the whole injection process lasts for very short time intervals through fast opening and closing of the needle valve. As the high-pressure fluid enters the nozzle discharge holes, cavitation may emerge due to sharp drop of the static pressure. The occurrence of cavitation in the nozzle and its significant effects on spray formation have been well known and extensively investigated [9]. However, experimental study of inside-nozzle-flow is tricky due to its small scale (0.1-0.2mm), high pressure (up to 1800 bar) and short switch intervals (within a few milliseconds). In order to facilitate clear visualisation of cavitation structure and laser measurement, larger-scale transparent nozzles have been widely adopted [10, 11, 12] in experiments instead of real ones. Few tests on real-size nozzles have been performed. Three-dimensional (3D) effects, which are believed to be important, cannot be visualised in real-size experiments [13, 14]. Besides, real-time measurements are difficult to achieve, either. Although having contributed valuable insights into the flow physics, these studies have, at the same time, revealed the complexity of the two-phase flow structures in the nozzle. Our understanding of the inside-injector flow physics is still far from sufficient, and accessing how it affects flow conditions at the nozzle exit is difficult, albeit crucial.

Numerical studies on this problem, which may play an important role in providing a detailed picture of inside-injector flow physics, are also limited due to methodology complexities. First, cavitating flow simulation is challenging using traditional approaches due to the presence of an interface between the liquid and vapour phases, which quickly changes its shape and where huge variations of the fluid properties occur [15], easily leading to nonphysical oscillations and instability without robust numerical schemes. Second, the needle movement needs to be dealt

with properly. Although body-fitted or unstructured grid methods have been commonly adopted to simulate moving boundary problems, the algorithms are generally complicated, in tandem with high computation costs.

Over the past three decades, the lattice Boltzmann method [1] based on mesoscopic fluid dynamics has attracted great attention due to its simple scheme, easement of dealing with complex geometry and convenience of parallel computing. From the physical essence, the kinetic behaviour of a multiphase flow system is the result of microscopic interactions among fluid phases. Based on the theory of molecular motion, LBM is especially suitable for simulating complex multiphase flow from first principles. In LBM computation, cavitation or phase transition will emerge spontaneously by using a multiphase model cooperating with an appropriate non-ideal equation of state (EOS) [16, 17]. Several multiphase LB models have been developed during the past two decades. The first so-called R-K model [18] was proposed by Gunstensen et al. in 1991, which uses colour gradients to separate the two fluid phases and model the interaction at multiphase interfaces. The pseudo-potential model, in which a pseudo-potential function is introduced to account for nonlocal particle interactions, was developed by Shan and Chen [4, 5, 6]. Other approaches such as the free energy model [19] and the mean-field model [20] were proposed in the following years. Overall, the Shan-Chen model has been most frequently employed in cavitation study due to its simplicity, high computational efficiency and high flexibility. It was for the first time used by Sukop and Or to simulate both homogeneous and heterogeneous cavitation with interface formation and bubble growth [21]. Falcucci et al. coupled the two-belt approach into the original Shan-Chen model, and a flow-induced incipient cavitation simulation was performed where cavitation bubbles emerged spontaneously [22]. Chen et al. [23] simulated the bubble growth with a large density ratio by coupling the exact difference method and the Carnahan-Starling real-gas equation of state into the Shan-Chen model.

Moving boundary problems can be relatively easily solved in LBM by its so-called no-slip treatment at a boundary. There are two main categories of no-slip boundary treatment in LBM. The first is known as the bounce-back scheme, which directly constructs the unknown distribution functions at boundary nodes using the known ones while complying with hydrodynamic constraints. The second is the immersed boundary method, which was proposed by Peskin [2, 3] in 1970s in order to simulate blood flow in the heart. This method was developed in conventional CFD framework, and can also be effectively and easily incorporated into LBM, since both the immersed boundary and LB methods are usually discretised on regular Cartesian mesh [24]. Both the bounce-back and immersed boundary methods have been extensively used by the LBM community in a wide range of applications. The immersed boundary method in general provides more stable solutions with an overall comparable accuracy and more convenience when dealing with complex geometry [25].

The objective of this study is to demonstrate that LBM is a potentially valuable tool to investigate complex flow inside a fuel injector where multiphase flow interacts with moving geometry. The immersed boundary method and Shan-Chen model are chosen to deal with the moving needle and cavitating flow, respectively. The open-source LB code Palabos [26] is used. Firstly, the accuracy and reliability of the immersed boundary method were tested by simulating an oscillating cylinder in a water tank [27] using LBM. Its movement is dictated by a sine function, which is similar to an injector needle. Then the Shan-Chen model capacity on simulating cavitating flow is assessed by the case of Sukop and Or [21] and a model injector without a needle. The remainder of the paper is structured as follows. In the next section, the immersed boundary method, Shan-Chen model and how they are coupled with LBM are introduced, followed by the simulation results and their comparisons against measurements and published numerical results [21, 28]. In the final section, the conclusions and future work are summarised.

Lattice Boltzmann Method

The LBM is based on the Boltzmann equation and simulates flow transport by the evolution of the distribution functions. The widely used Bhatnagar-Gross-Krook (BGK) approximation [1] for incompressible flow is employed in the present study. The BGK method is based on the development of discrete molecular velocity distribution functions on uniform Cartesian lattices. The velocity distribution functions can be written as

$$f_i(\mathbf{x}+\mathbf{e_i}\delta t, t+\delta t) - f_i(\mathbf{x},t) = -\frac{\delta t}{\tau}[f_i(\mathbf{x},t) - f_i^{\mathrm{eq}}(\mathbf{x},t)] + \left(1-\frac{1}{2\tau}\right)F_i(\mathbf{x},t)\delta t, \tag{1}$$

$$f_i^{\mathrm{eq}} = \omega_i \rho \left[1 + \frac{\mathbf{u}\cdot\mathbf{e_i}}{c_\mathrm{s}^2} + \frac{(\mathbf{u}\cdot\mathbf{e_i})^2}{2c_\mathrm{s}^4} - \frac{\mathbf{u}\cdot\mathbf{u}}{2c_\mathrm{s}^2}\right], \tag{2}$$

$$\rho = \sum_i f_i, \quad \rho\mathbf{u} = \sum_i f_i \mathbf{e_i} + \frac{\mathbf{F}\delta t}{2}, \quad \nu = (\tau - 0.5)c_\mathrm{s}^2\delta t, \tag{3}$$

where f and f^{eq} are the distribution function and equilibrium distribution function, respectively; the index i defines the vector of the discrete molecular velocities; ω is the weight factor for different speed vectors; τ and ν are the relaxation time and kinematic viscosity, respectively; c_s is the lattice speed of sound, and its squared value usually equals $1/3$; $\mathbf{u}$ and ρ are the macroscopic velocity and density, respectively; $\mathbf{x}$ and $\mathbf{e}$ are the spatial location and base velocity in the LBM, respectively; $\mathbf{F}$ is the external force and determined by Guo's scheme [29],

$$F_i(\mathbf{x},t) = \mathbf{F}\cdot\omega_i\left[\frac{\mathbf{e_i}-\mathbf{u}}{c_\mathrm{s}^2} + \frac{(\mathbf{e_i}\cdot\mathbf{u})\mathbf{e_i}}{c_\mathrm{s}^4}\right]. \tag{4}$$

Immersed boundary method

The immersed boundary method was firstly incorporated into LBM by Feng and Michaelides [30] in 2004. The basic idea of this method is to approximate a boundary by a set of off-lattice maker points that affect the fluid via a force. An interpolation stencil is introduced to couple the lattice and the maker points. There are several approaches of how to calculate the force, such as the penalty feedback forcing [30], direct forcing [31] and momentum exchange forcing [32]. Among them, the direct forcing method has been extensively used due to its simple scheme and numerical stability, and therefore has been used in the present research. The direct forcing algorithm and its incorporation into LBM are introduced as follows:

1. The velocity $\mathbf{u}$ on the Eulerian grid $\mathbf{x}$ is interpolated onto the Lagrangian gird $\mathbf{X}$ using Equation 5 to obtain the velocity $\mathbf{U}$ on the Lagrangian grid

$$\mathbf{U}(\mathbf{X}) = \sum_{\mathbf{x}} \mathbf{u}(\mathbf{x})\delta_h(\mathbf{x}-\mathbf{X})h^3, \tag{5}$$

where h^3 and δ_h are the volume of a Eulerian grid cell and the interpolation kernel function [33], respectively. We use the three-point delta-function to determine δ_h:

$$\delta_h = \frac{1}{h^2}\phi\left(\frac{x}{h}\right)\phi\left(\frac{y}{h}\right), \quad \phi(r) = \begin{cases} \frac{1}{3}\left(1+\sqrt{1-3r^2}\right) & 0 \le |r| \le \frac{1}{2} \\ \frac{1}{6}\left(5-3|r|-\sqrt{-2+6|r|-3r^2}\right) & \frac{1}{2} < |r| \le \frac{3}{2} \\ 0 & \frac{3}{2} < |r| \end{cases}. \tag{6}$$

2. The boundary force $\mathbf{F}_\mathrm{b}(\mathbf{X})$ used to enforce the no-slip condition on the Lagrangian grid is calculated as

$$\mathbf{F}_\mathrm{b}(\mathbf{X}) = \frac{\mathbf{U}_\mathrm{b}(\mathbf{X}) - \mathbf{U}(\mathbf{X})}{\delta t}, \tag{7}$$

where $\mathbf{U}_\mathrm{b}(\mathbf{X})$ is the macroscopic velocity of the moving object. In our case, it is the needle velocity.

3. The boundary force is then distributed back onto the Eulerian grid by

$$\mathbf{f}_\mathrm{b}(\mathbf{x}) = \sum_{\mathbf{X}} \mathbf{F}_\mathrm{b}(\mathbf{X})\delta_h(\mathbf{x}-\mathbf{X})\Delta V, \tag{8}$$

where ΔV is the control volume of a Lagrangian grid cell, which is usually given the same value of h^3.

4. Compute the uncorrected (pre-collision) velocity $\mathbf{u}_n(\mathbf{x},t)$ from Equation 9. Then obtain $F_i(\mathbf{x},t)$ in Equation 1 from $\mathbf{f}_\mathrm{b}(\mathbf{x})$ through Guo's scheme [29] (Equation 4), and perform LB algorithms with Equations 1, 2, 3 and 4. The updated velocity $\mathbf{u}_{n+1}$ on the Eulerian grid is then obtained by Equation 10:

$$\mathbf{u}_n = \frac{\sum_i f_i \mathbf{e_i}}{\rho}, \tag{9}$$

$$\mathbf{u}_{n+1}(\mathbf{x}) = \mathbf{u}_n(\mathbf{x}) + \frac{\mathbf{f}_\mathrm{b}(\mathbf{x})\delta t}{2\rho}. \tag{10}$$

5. Update the position of the moving object and perform the same cycle in the next time step.

Shan-Chen pseudo-potential method for single-component fluid

In order to introduce nonlocal interaction among particles, Shan and Chen [4, 5, 6] defined a force ($\mathbf{F}^\mathrm{SC}$) which is modelled by a sum of pseudo-potential interactions with the nearest lattice neighbours, as shown in Equation 11. We also use Guo's scheme to incorporate this force into Equation 1, similar to what is done in the immersed boundary method.

$$\mathbf{F}^\mathrm{SC}(\mathbf{x},t) = -\Psi(\rho)G\sum_i \omega_i \Psi(\mathbf{x}+\mathbf{e_i}\delta t)\mathbf{e_i}\delta t, \tag{11}$$

where G is a simple scalar that controls the strength of the interaction. The force is attractive for negative values and repulsive for positive ones. $\Psi(\rho)$ is the pseudo-potential function, for which several forms have been proposed [4, 5, 6]. Two of them are chosen in the present study, i.e.

$$\Psi(\rho) = \rho_0[1-\exp(-\rho/\rho_0)], \tag{12}$$

$$\Psi(\rho) = \Psi_0\exp(-\rho/\rho_0), \tag{13}$$

where Ψ_0 and ρ_0 are arbitrary constants. Through a third-order Taylor expansion and simple merging, Equation 11 can be written as

$$\mathbf{F}^\mathrm{SC}(\mathbf{x},t) = -G\Psi(\rho)\left[c_\mathrm{s}^2\delta t^2\nabla\Psi(\rho) + \frac{c_\mathrm{s}^4\delta t^4}{2}\nabla\Delta\Psi(\rho)\right]. \tag{14}$$

So, the two major features of non-ideal fluids are captured, namely, a non-ideal equation of state relating to the first term and surface tension relating to the second term on the right-hand side of Equation 14. The correction to the ideal EOS $p = \rho c_\mathrm{s}^2$ due to the introduction of this force leads to the following non-ideal EOS,

$$p = \rho c_\mathrm{s}^2 + \frac{G c_\mathrm{s}^2 \delta t^2}{2}\Psi^2(\rho). \tag{15}$$

Simulation results and discussion

Validation for immersed boundary method

The needle in a fuel injector oscillates, leading to the injector switching between opening and closing continuously. This motivated us to validate the immersed boundary method against Dütsch's measurements [27], in which a cylinder oscillates according to a sine function (Figure 1).

Two dimensionless parameters, i.e. the Reynolds number and Keulegan-Carpenter number, are defined as

$$Re = U_{\max} D/\nu, \quad KC = U_{\max}/vD, \tag{16}$$

where $U_{\max}$ and D are the maximum velocity and cylinder diameter, respectively. And ν and v denote the kinematic viscosity and characteristic frequency, respectively. In the present study, $Re = 100$ and $KC = 5$.

The cylinder motion is specified by

$$X_{\text{cen}}(t) = -\frac{1}{2\pi}\sin(2\pi v t), \tag{17}$$

where X_{cen} is the x coordinate of the cylinder centre. In our simulation, a uniform Cartesian mesh is constructed for a domain of $50D$ and $30D$ ($D = 25\Delta x$) in the x and y directions, and the initial location of the cylinder is at the centre of the domain. The Neumann boundary condition is used at the outer boundary, i.e. zero velocity gradient. Figure 2 shows the velocity profiles at four different x locations ($x = -0.6D$, $0D$, $0.6D$ and $1.2D$) for three different phase angles (a) $\phi = 2\pi f t = 180^\circ$, (b) $\phi = 210^\circ$, and (c) $\phi = 330^\circ$. It can be seen that the present results have overall good agreements with the experimental data. It is expected that the velocity distribution should be symmetric and antisymmetric for the u and v velocities, respectively, along the y direction [34]. So, discrepancies at comparisons where the experimental data are neither symmetric nor antisymmetric are due to measurement uncertainty.

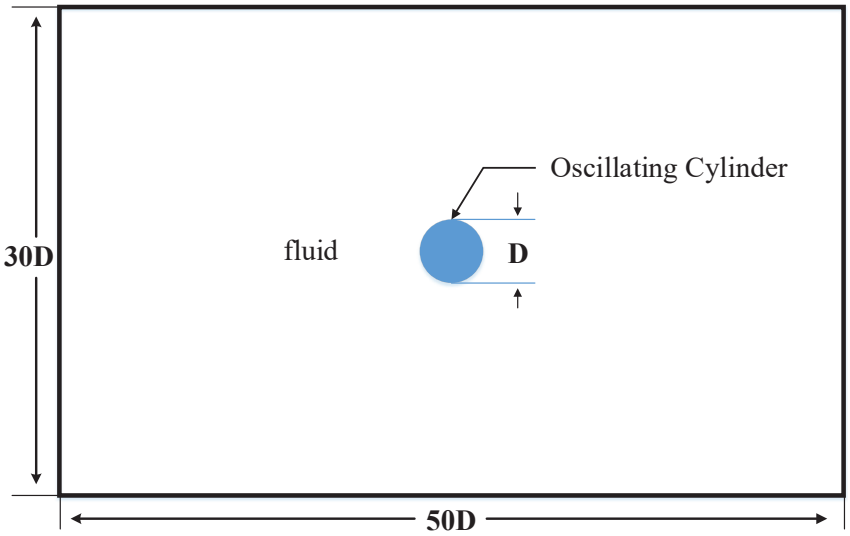

Figure 1. Computation sketch of oscillating cylinder.

Validation for cavitating flow

Spinodal decomposition We started our validation of cavitating flow from a simple case, which is known as the first cavitating flow simulation by LBM and investigated by Sukop and Or [21] in 2005. The simulation was conducted in a 200×200 domain, with periodic boundaries at the top and bottom and constant normal outflow velocity boundary (0.005) at the left and right. This leads to the increase of tension in liquid with time until the liquid spinodal pressure and density are reached, then the liquid cavitates catastrophically. Equation 13 is chosen as the pseudo-potential function and the initial density in the domain is 400, which are in accordance with the setup of Sukop and Or. Figure 3 shows the density variations at two points during the course of 12,000 time steps. As shown in the plot, severe fluctuations occur after the onset of cavitation, and the densities at the two monitored locations eventually reach their equilibrium, flat, free interface values, with the liquid density being 524 and the vapour density 85. The overall agreements are good between the two results, with little discrepancy existing. The viscosity value was not given by Sukop and Or in their paper, and we set it to be 0.25.

Cavitating flow in a model nozzle In the present study, the nozzle flow simulation was performed by using the same model and parameters of Falcucci et al. [28], as shown in Figure 4. In our simulation, the velocity inlet boundary condition with a magnitude of 0.13 was set, and the Neumann boundary condition was used at the outlet. The initial conditions, which are important for the unsteady simulation and comparison, are 0.13 for velocity and 1.91 for density, respectively.

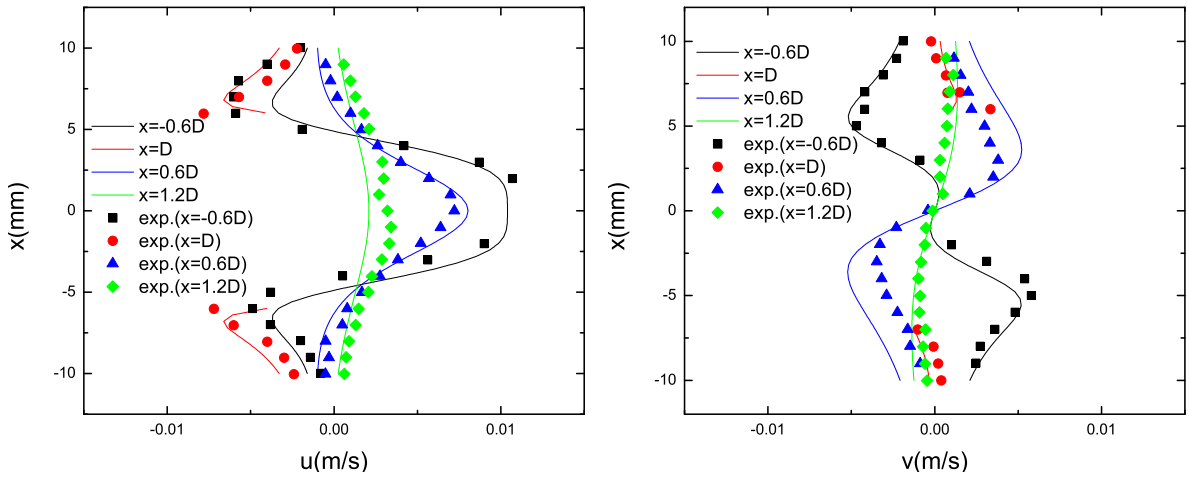

(a) u at $\phi = 180^\circ$ (b) v at $\phi = 180^\circ$

(c) u at $\phi = 210^\circ$ (d) v at $\phi = 210^\circ$

(e) u at $\phi = 330^\circ$ (f) v at $\phi = 330^\circ$

Figure 2. Velocity profiles for three different phase angles $\phi = 180^\circ$, 210° and 330°. Lines are the present simulation results, while symbols are the experimental results of Dütsch et al. [27].

Figure 5 shows the comparisons of density contours at three time instants, and it can be seen that satisfactory agreements have been obtained. In the nozzle, due to the sudden reduction of flow area at the sack wall corner, the liquid flow experiences a pressure drop caused by the acceleration, which triggers cavitation eventually. The formation of a cavitation bubble and its growth are clearly visible. It indicates that Shan-Chen model has the ability to capture flow-induced cavitation. There are, however, inherent limitations in the original Shan-Chen model. For instance, the maximum density ratio between liquid and vapour is about 50, which restricts the application of the model in realistic gas-liquid two-phase flow systems. This motivates us to further develop the model in future work.

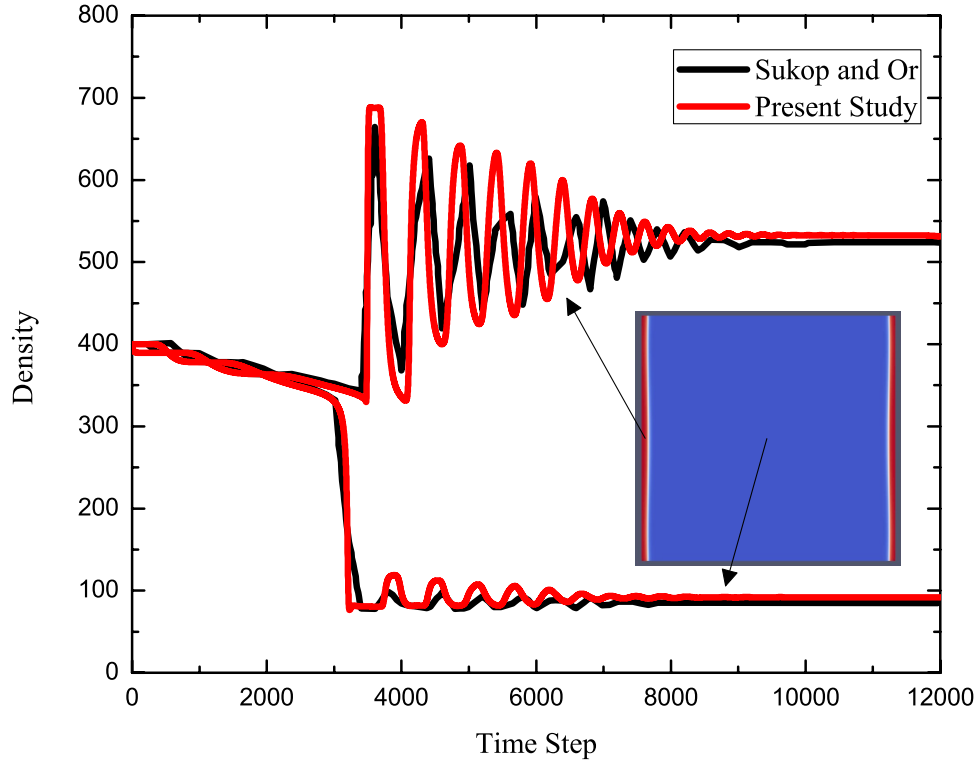

Figure 3. Density variations at two monitored locations against time. The fluid phase at (100,100) turns into vapour and remains liquid at (1,100).

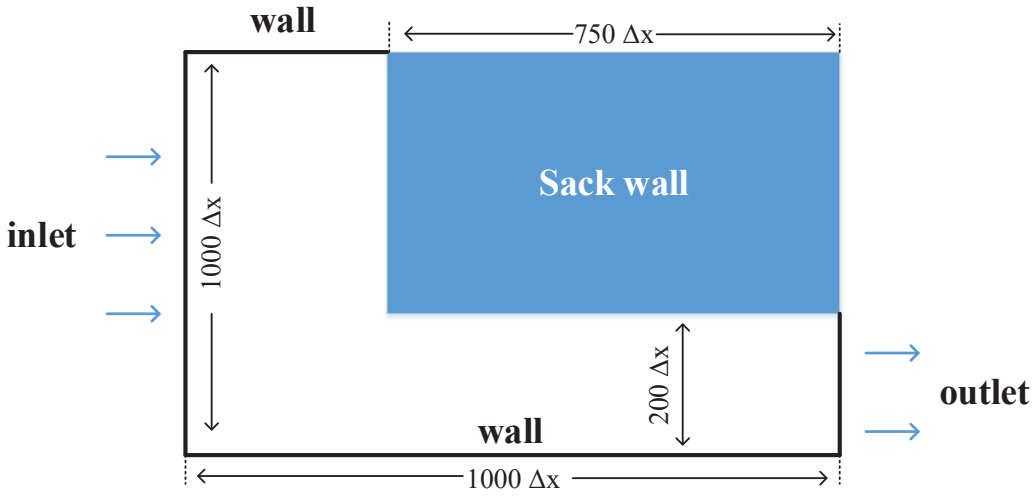

Figure 4. Sketch of model nozzle.

Conclusions and future work

In the present study, a preliminary investigation towards better understanding flow dynamics in a model fuel injector was conducted using the open-source LB code Palabos. The immersed boundary method and Shan-Chen multiphase model were adopted and will be further developed to target on simulating the needle movement and cavitating flow inside the injector. Both methods were validated under the framework of LBM. Firstly, the immersed boundary method was validated by simulating the flow around an oscillating cylinder, which moves according to a similar algorithm to a real needle, and good agreement between the numerical and experimental results was obtained. Then the Shan-Chen model was validated against published data [21, 28], and results indicate it is a promising model to simulate cavitating flow, although limitations, e.g. on the maximum liquid/vapour density ratio which can be tolerated by the model, exist.

Our future work firstly aims at further development of the Shan-Chen model, making it suitable for simulating two-phase flow with a larger density ratio and normal ambient temperature as in real fluid. Then the immersed boundary method and Shan-Chen model will be collaboratively incorporated into LBM. Our long-term objective is to analyse flow dynamics inside a realistic fuel injector where multiphase flow interacts with moving geometry using LBM. Further development of the mesoscopic numerical approach can benefit a variety of engineering, materials

and medical spraying applications in which the working-liquid injector is a key component to determine the spray performance.

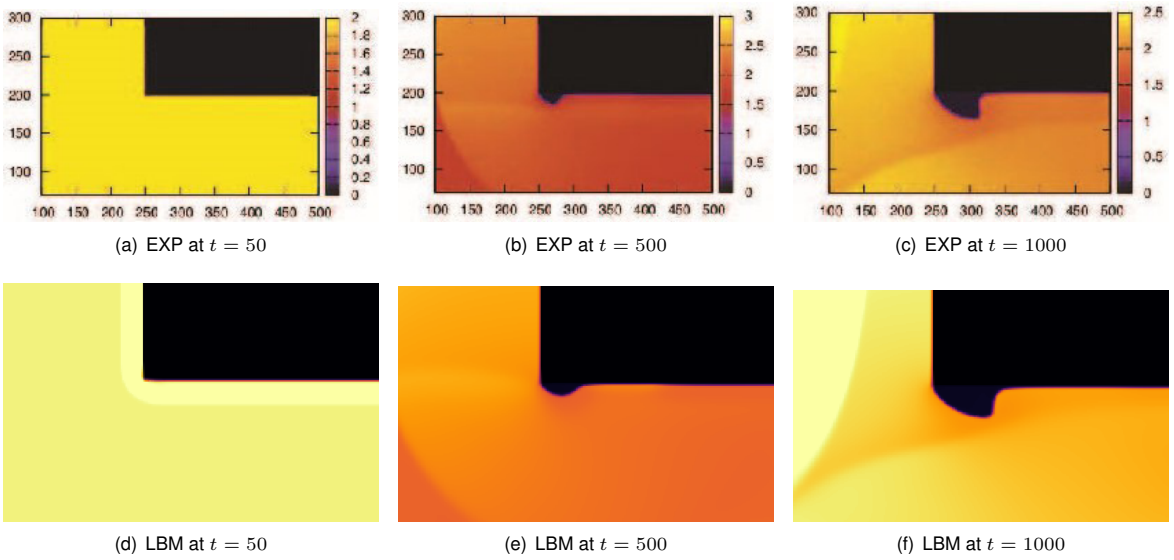

(a) EXP at $t = 50$ (b) EXP at $t = 500$ (c) EXP at $t = 1000$

(d) LBM at $t = 50$ (e) LBM at $t = 500$ (f) LBM at $t = 1000$

Figure 5. Density-contour comparisons at t = 50, 500 and 1000 between the present study (bottom row) and [34].

Acknowledgements

This work was performed by the first author TPL as a visiting researcher at Brunel University London. The authors gratefully acknowledge the financial support from the China Scholarship Council (No. CSC201804980019).

Nomenclature

c_s	lattice sound speed
D	cylinder diameter
$\mathbf{e}$	lattice base velocity
f	distribution function
$\mathbf{f}_\mathrm{b}$	boundary force on Eulerian grid
f^eq	equilibrium distribution function
$\mathbf{F}$	external force
$\mathbf{F}_\mathrm{b}$	boundary force on Lagrangian grid
F_i	force term in Guo's scheme
$\mathbf{F}^\mathrm{SC}$	pseudo-potential interaction force
G	interaction strength parameter
h^3	volume of a Eulerian grid
i	vector of the discrete molecular velocities
KC	Keulegan-Carpenter number
p	pressure
Re	Reynolds number
t	time
$\mathbf{u}$	macroscopic velocity on Eulerian grid
$\mathbf{U}$	macroscopic velocity on Lagrangian grid
$\mathbf{U}_\mathrm{b}$	macroscopic velocity of the moving object
U_max	maximum velocity of cylinder
v	characteristic frequency of cylinder
$\mathbf{x}$	spatial location on Eulerian grid
$\mathbf{X}$	spatial location on Lagrangian grid
X_cen	x coordinate of cylinder centre
δ_h	interpolation kernel function
δt	time step
ΔV	control volume of a Lagrangian grid
Δx	lattice grid spacing
ν	kinematic viscosity
ρ	density
ρ_0	density parameter in pseudo-parameter function
τ	relaxation time
$\phi(r)$	three-point delta function

Ψ_0 pseudo-potential function parameter
$\Psi(\rho)$ pseudo-potential function
ω weight factor

References

[1] Chen, S. Y., Doolen, G. D., 1998, *Annual Review of Fluid Mechanics*, 30, pp. 329-364.
[2] Peskin, C. S., 1972, *Journal of Computational Physics*, 10 (2), pp. 252-271.
[3] Peskin, C. S., 1977, *Journal of Computational Physics*, 25 (3), pp. 220-252.
[4] Shan, X. W., Chen, H. D., 1993, *Physical Review E*, 47 (3), pp. 1815-1819.
[5] Shan, X. W., Chen, H. D., 1994, *Physical Review E*, 49 (4), pp. 2941-2948.
[6] Shan, X., Doolen, G., 1995, *Journal of Statistical Physics*, 81 (1-2), pp. 379-393.
[7] Payri, R., García, J. M., Salvador, F. J., Gimeno, J., 2005, *Fuel*, 84 (5), pp. 551-561.
[8] Suh, H. K., Chang, S. L., 2008, *International Journal of Heat & Fluid Flow*, 29 (4), pp. 1001-1009.
[9] Giannadakis, E., Gavaises, M., Arcoumanis, C., 2008, *Journal of Fluid Mechanics*, 6 (16), pp. 153-193.
[10] Sou, A., Hosokawa, S., Tomiyama, A., 2007, *International Journal of Heat & Mass Transfer*, 50 (17), pp. 3575-3582.
[11] He, L., Ruiz, F., 1995, *Atomization and Sprays*, 5 (6), pp. 569-584.
[12] Henry, M. E., Collicott, S. H., 2000, *Atomization and Sprays*, 10 (6), pp. 545-563.
[13] Chaves, H., Knapp, M., Kubitzek, A., Obermeier, F., Schneider, T., 1995, *Journal of Engines*, 104 (3), pp. 645-657.
[14] Badock, C., Wirth, R., Fath, A., Leipertz, A., Jul. 6.-8. 1998, 14th European Conference on Liquid Atomization and Spray Systems.
[15] Kahler, G., Bonelli, F., Gonnella, G., Lamura, A., 2015, *Physics of Fluids*, 27 (12), article no. 123307.
[16] Sofonea, V., Lamura, A., Gonnella, G., Cristea, A., 2004, *Physical Review E*, 70 (4), article no. 046702.
[17] Gonnella, G., Lamura, A., Sofonea, V., 2007, *Physical Review E*, 76 (3), article no. 036703.
[18] Gunstensen, A. K., Rothman, D. H., Zaleski, S., Zanetti, G., 1991, *Physical Review A*, 43 (8), pp. 4320-4327.
[19] Swift, M. R., Orlandini, E., Osborn, W. R., Yeomans, J. M., 1996, *Physical Review E*, 54 (5), pp. 5041-5052.
[20] He, X., Shan, X., Doolen, G. D., 1998, *Physical Review E*, 57 (1), pp. 13-16.
[21] Sukop, M. C., Or, D., 2005, *Physical Review E*, 71 (4), article no. 046703.
[22] Falcucci, G., Jannelli, E., Ubertini, S., Succi, S., 2013, *Journal of Fluid Mechanics*, 728, pp. 362-375.
[23] Chen, X. P., Zhong, C. W., Yuan, X. L., 2011, *Computers and Mathematics with Applications*, 61, pp. 3577-3584.
[24] Zhu, L. D., He, G. W., Wang, S. Z., Miller, L., Zhang, X., You, Q., Fang, S., 2011, *Computers and Mathematics with Applications*, 61 (12), pp. 3506-3518.
[25] DeRosis, A., Ubertini, S., Ubertini, F., 2014, *Journal of Scientific Computing*, 61 (3), pp. 477-489.
[26] Palabos, http://www.palabos.org/ ([cit. 2019-03-24]).
[27] Dütsch, H., Durst, F., Becker, S., Lienhart, H., 1998, *Journal of Fluid Mechanics*, 360, pp. 249-271.
[28] Falcucci, G., Ubertini, S., Bella, G., Succi, S., 2013, *Communications in Computational Physics*, 13 (3), pp. 685-695.
[29] Guo, Z., Zheng, C., Shi, B., 2002, *Physical Review E*, 65, article no. 046308.
[30] Feng, Z. G., Michaelides, E. E., 2004, *Journal of Computational Physics*, 195 (2), pp. 602-628.
[31] Feng, Z. G., Michaelides, E. E., 2005, *Journal of Computational Physics*, 202 (1), pp. 20-51.
[32] Niu, X., Shu, C., Chew, Y., Peng, Y., 2006, *Physics Letters A*, 354 (3), pp. 173-182.
[33] Peskin, C. S., 2002, *Acta Numerica*, 11, pp. 479-517.
[34] Liao, C. C., Chang, Y. W., Lin, C. A., McDonough, J. M., 2010, *Computers and Fluids*, 39 (1), pp. 152-167.